Solar selective coatings based on Carbon:Transition Metal Nanocomposites

Irene Heras*[a], Elena Guillén[a], Matthias Krause[b], Ainhoa Pardo[c], Jose L. Endrino[d], Ramón Escobar Galindo[a]

[a] Abengoa Research S. L., Abengoa, Seville, Campus Palmas Altas 41014, Spain [b] Helmholtz Zentrum Dresden Rossendorf, Dresden, Germany. [c] Centre Tecnologic de Manresa, Manresa, Spain. [d] School of Aerospace, Transport, and Manufacturing, Cranfield University, United Kingdom

ABSTRACT

The design of an efficient and stable solar selective coating for Concentrating Solar Power central receivers requires a complex study of the materials candidates that compose the coating. Carbon-transition metal nanocomposites were studied in this work as absorber materials because they show appropriate optical properties with high absorption in the solar region and low thermal emittance in the infrared. Furthermore metal carbides are thermal and mechanical stable in air at high temperatures.

In this work a solar selective coating was grown by a dual source filtered cathodic vacuum arc. The complete stack consists on an infrared reflection layer, an absorber layer of carbon-zirconium carbide nanocomposites and an antireflection layer. The aim of this research is optimize the absorber layer and for that, the metal content was controlled by adjusting the pulse ratio between the two arc sources. The elemental composition was determined by Ion Beam Analysis, X-Ray diffraction measurements show the crystal structure and the optical properties were characterized by spectroscopic ellipsometry measurements. The reflectance spectra of the complete selective coating were simulated with the optical software CODE. Bruggeman effective medium approximation was employed to average the dielectric functions of the two components which constitute the nanocomposite in the absorber layer. The optimized coating exhibited a solar absorptance of 95.41% and thermal emittance of 3.5% for 400ºC. The simulated results were validated with a deposited multilayer selective coating.

Keywords: Solar selective coatings, carbide thin films, high temperature applications, cathodic arc deposition, optical simulation

1. INTRODUCTION

The search of new absorber coatings is of crucial interest to Concentrating Solar Power (CSP) companies for the new design of advanced receivers. Different alternatives to commercial absorber paints are being searched due to the degradation problems they show at high temperatures when exposed at air.

Physical Vapor Deposition (PVD) techniques have been proven to be an excellent alternative for the deposition of selective coatings with high absorptance (α >90%) and low emittance (ε < 30) for temperatures up to 400ºC in parabolic trough concentrated solar power applications[1]. Different PVD techniques has been successfully employed to deposit solar selective coating such as magnetron sputtering[2], laser sintering[3], ion beam co-sputtering[4] or filtered cathodic vacuum arc (FCVA)[5]. Among those different processes, FCVA processes the highest ionization ratio, which ensures dense thin films with a better adhesion between the substrate and the coating. FCVA can be applied to large area and non-planar substrates such as cylinders or tubes, typical geometry of the current receivers.

Most solar selective coatings use ceramic-metal composites (cermets) such as Co:Al_2O_3[6], Mo:Si_3N_4[7] or Ni:SiO_2[2]. All those absorber coatings exhibit high stability and corrosion resistant properties, but fails at temperatures higher than 400ºC. The improvements in efficiencies for solar thermal energy conversions partially mean the increase in the receivers' temperature, reaching up to an average maximum temperature of 650ºC for superheated steam and molten salts receivers, so alternative materials are needed.

The interstitial carbides are stable materials at temperature above 1000ºC with high reflectivity due to their metallic character. While Carbon-Transition Metal nanocomposite (C:TM) show optical selective properties [8] (low reflectance in the visible wavelength range and high reflectance in the infrared range). These properties make C:TM very attractive materials for applications where high temperature resistant and selective optical properties are required, for instance thermal solar energy applications.

Previous attempts of depositing C:TM for solar selective coatings can be found in the literature [9,10]. In most of those examples, the C:TMs have similar degradation mechanisms: diffusion of the substrate or intermediate layers along the absorber layer, oxidation of the metal carbide component or graphitization of the amorphous carbon component. Those problems can be solved employing FVCA deposition technique and an appropriate antireflection - protective oxide layer on the top of the selective coating.

The computer program CODE was used to simulate the reflectance spectra of a complete solar selective coating, consisting of an infrared reflection (IR) layer between the substrate and the coating, highly reflective in the infrared range to minimize thermal loses; the C:TM absorber layer and a antireflection (AR) layer. The AR layer can be a ceramic or dielectric material like Al_2O_3 or SiO_2, and must have a double utility: be transparent to solar radiation and protect the whole coating to reduce the corrosion rate and stabilize the coating at high temperatures.

The optical properties of the materials employed in the simulations can be measured or taken from literature. For the C:TM, as inhomogeneous materials, the optical properties can be described by so-called effective medium approximations (EMA). Macroscopically the inhomogeneity cannot be detected and the system can be treated then as being quasi-homogeneous. An EMA ε_{eff} can be introduced, which is a non-trivial average of the dielectric functions of the individual components of the nanocomposite. Several mixing formulas have been established, being the most prominent the ones of Maxwell Garnett[11], Bruggeman[12] and Bergman[13]. The Bergman is the most general form of effective medium approaches but is necessary further information about the composite, the so-called function spectral density, not easy to obtain without experimental data. Maxwell-Garnett theory, assumes that the medium has a separated grain structure and it is applicable only to systems of low volume of embedded particles, so it cannot be applied for this C:TM where percolation normally occurs. Therefore, Bruggeman effective medium theory is a good choice for analyzing the optical properties for the nanocomposite absorber layer.

The simulations allow us to predict the optical properties of the complete coating without the necessity of deposit all the possible alternatives. Several parameters can be modified easily within the simulation: the thickness of the different layers, the number of layers that compose the complete coating or the different metal content in the nanocomposite.

In this work a-C:ZrC has been selected as absorber layer of the solar selective coating and different combinations were deposited by FVCA. After the deposition of single layers, the elemental composition of the samples was determined by Rutherford Backscattering Spectrometry (RBS) and Nuclear Reaction Analysis (NRA), the crystal structure was studied with X-ray diffraction (XRD) and the optical properties have been characterized by spectroscopic ellipsometry (SE). Scanning Electron Microscopy (SEM) was employed to observe the micro-structure of the deposited thin films. Using the measured optical constants, a batch of simulations was done, with the final selection of the best candidate to be deposited as solar selective coating for high temperature applications.

2. EXPERIMENTAL DETAILS

Thin films were grown on Si (100) and on polished Inconel HAYNES 625 substrates using a pulsed FCVA, from Plasma Technology Limited, Hong Kong[14]. Before the deposition, the substrates were cleaned by ultrasound in distilled water, acetone and ethanol.

This system is provided with two pulsed filtered cathodic arc sources to reduce the incorporation of macroparticles in the growing films. The generated arc plasmas created into the filters are guided into the vacuum chamber by an electromagnetic field applied to the curved ducts. External solenoid coils are wrapped around the ducts and produce an axial magnetic field of about 200 G. The coils are biased 20 V with a current of 15 A to build up a lateral electrical field.

The substrates were situated in a rotating holder 240 mm away from the exit of the duct, in the center of the camber. A negative pulsed bias voltage of −400 V (100 KHz, 20% duty cycle) was applied to the substrates during film deposition. Figure 1 shows the schematic diagram of the PFCVA system employed for the film deposition. The samples were rotated constantly with a rotation speed of 1.4 rpm. The deposition chamber was evacuated to a vacuum of about $2 \cdot 10^{-3}$ Pa before deposition. During film deposition, an argon flow of 3.5 sccm was introduced into the chamber to stabilize the arc, and the working pressure was kept at 0.11 Pa through a pressure control valve. The cathodes were ignited using discharge pulse duration of 3 ms at a repetition rate of 7.5 Hz.

Carbon-zirconium samples were prepared by the co-evaporation of C and Zr, using the two cathodic arc sources, one provided with a carbon cathode and the second arc source with pure metallic zirconium cathode. The deposition process time of all the samples was 30 minutes. To vary the metal content on the thin film, the ratio of the main current applied to each one of the cathodes can be modified. The intensity of the carbon arc source was kept constant of 2.5A in all cases while the current ratio of the metallic arc cathode was varied from 1.25 to 5A.

The thickness and roughness of the deposited samples has been measured by using a 50x objective Confocal Microscope Plμ 2300 de Sensofar.

The film areal densities were determined by combined RBS and NRA measurements. To obtain elemental composition, samples deposited on Silica substrate were employed for this analysis. RBS was realized with 2MV Van der Graff accelerator and NRA was performed with the 3 MeV tandem accelerator, both facilities at Helmholtz Zentrum Dresden-Rossendorf (HZDR) in Germany. The RBS spectra were collected with $^{4+}$He ions with an energy beam of 1.7 MeV. The data were acquired with a silicon barrier detector located at a backscattering angle of 170º, with an energy detector resolution of 13 keV. The simulation software SIMNRA[15] version 6.06 was used to determine the composition. The NRA measurements were used to accurately determine the amount of carbon. For that aim we employed deuterium ions as incident particles with energy of 1.248 MeV and a detection angle of 135º. The nuclear reaction $^{12}C(d,p)^{13}C$ cross section exhibits its maximum for this deuterium ion energy approximately, significantly enhancing the proton signal from the carbon atoms[16] . Simultaneously, RBS of deuterium from the heavier metallic atoms provide us the metal content of each one of the deposited layers. The areal densities were estimated using surface approximation from the integrals of the metal and the carbon peaks.

The phase structure and crystallinity of the dispersed phase in the thin films were investigated by XRD with grazing incidence diffraction (GID) geometry using a PANalytical X'Pert PRO diffractometer with Cu-K_α radiation (λ=1.542 Å). The incident angle was 0.4º, and the XRD patterns were measured in the diffraction angle 2θ range of 30–100º in steps of 0.05º. The patterns are intermitted between ~50 and 53º in order to blind the intense peak at ~52º, attributed to the Si (100) substrate, which is observed in all the patterns.

The optical constants of the C:TM thin films in the wavelength range of 200 to 1700 nm at an angle of polarized light incidence of 75º were determined by SE using rotating compensator ellipsometer M -2000 FI (J. A.Woolam, Inc). The data were acquired and interpreted via modeling using WVASE32® software, version 3.6[17] .

Cross section images of the complete deposited film were taken with a SEM Zeiss Utrapluss, operating at 10kV accelerating voltage.

The computer software CODE[18] has been employed to calculate the reflectance spectra of a complete solar selective coating, without the requirement of depositing it. The optical coatings of the single layer were obtained from measured single layers. To simulate the optical constants of the inhomogeneous nanocomposite, Bruggeman[12] EMA was employed, which equation is:

$$(1-f)\frac{\varepsilon_M - \varepsilon_{eff}}{\varepsilon_M + 2\,\varepsilon_{eff}} + f\frac{\varepsilon - \varepsilon_{eff}}{\varepsilon + 2\,\varepsilon_{eff}} = 0 \qquad (1)$$

Where $\mathcal{E}_M$ is the dielectric function of the matrix material, $\mathcal{E}$ is the dielectric function of the particles, and f is the volume fraction of particles embedded in the composited.

After the corroboration that the EMA can be valid for both this type of nanocomposite, we proceeded to optimize the values of the metal content and thicknesses to search the combination of parameters which provide the best solar absorptance and thermal emittance. The solar absorptance (α) of a solar selective coating is defined as the fraction of incident radiation at a wavelength that is absorbed, following the ASTM G173[19], as defined equation (2):

$$\alpha = \frac{\int_{\lambda_1}^{\lambda_2}[1-R(\lambda)]G(\lambda)d\lambda}{\int_{\lambda_1}^{\lambda_2}G(\lambda)d\lambda} \quad (2)$$

where λ_1=300 nm and λ_2 = 2500 nm denote the lower and upper solar wavelengths, $R(\lambda)$ the total reflectance, and $G(\lambda)$ is the reference solar spectrum AM1.5.

The Thermal emittance (ε_T) is obtained from the reflectance spectra, and applying Kirchoff´s law, as described in equation (3), for each temperature *T*.

$$\varepsilon_T = \frac{\int_{\lambda_1}^{\lambda_2}[1-R(\lambda,T)]B(\lambda,T)d\lambda}{\int_{\lambda_1}^{\lambda_2}B(\lambda,T)d\lambda} \quad (3)$$

where λ_1=2500 nm and λ_2 = 30000 nm are the wavelength range to calculate the effective thermal emittance and $B(T,\lambda)$ is the spectral blackbody radiation at an specific temperature *T,* given by Planck's law[20] .

3. RESULTS AND DISCUSSION

RBS and NRA analysis were performed to determine the metal and carbon ratio and also the presence of other constituents. As show Figure 1, the RBS spectra have a thick step assigned to the silicon substrate, and the carbon signal overlaps of that silicon. For this motive, NRA measures are necessary to have a precise determination of the carbon concentration.

RBS analysis was done for calculating the areal density of the metal (10^{15} atoms/cm^2) and only one spectrum is necessary for calibrating the equivalent areal density of the Zr. Then experimental spectra were fitted with SIMNRA [15]

A small peak is appreciated around 1100 keV, due to Ar content of less than 3%. The presence of Ar can be explained because an Ar flow was introduced during the deposition in order to stabilize the arc formation. A little concentration of a metal heavier than Zr can be appreciated, probably Hafnium, in a content lower than 0.5% which is a typical impurity of commercial Zr cathodes.

All the C-Zr deposited samples were analysed by NRA (results not shown). With the RBS Zr content calibration, the atomic % of metal and carbon have been accurately established. We obtain 16 ±1 at% of Zr for the low metal content sample and 48 ±1 at. % Zr for the deposited sample with high metal content.

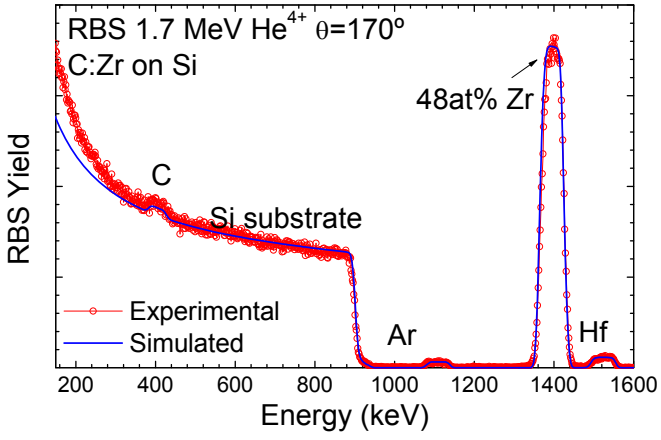

Figure 1. RBSspectra C:Zr thin films with high metal content.

Figure 2 shows the X-ray patterns of two C-Zr thin films grown on Si (100) substrate. The fcc ZrC main peaks are shown in the figure. In the XRD pattern of the sample with low Zr content (16 at.% Zr), no peaks are observed and the metal atoms are distributed in the carbon matrix without significant formation of any crystal, indicating its amorphous character. However in the case of the C-Zr sample with 48at.%Zr, the crystallinity increases as revealed by the appearance of one well-defined Bragg peak situated at $2\theta \approx 33^{\circ}$ assigned to the (111) plane of ZrC fcc – like structure (ICDD card number 00-019-1487)[21]. An estimation of the crystal size was done employing the Scherrer formula from the XRD pattern, and we obtain a crystal size of 2.2 nm for the (111) lattice plane.

The apparition of the sharp peak at $2\theta \approx 43^{\circ}$ in the 48 at.% Zr sample, cannot be attributed to any zirconium carbide or zirconium metallic crystal formation. This peak become visible due to scattering from the amorphous carbon, as is also shown by Adelhelm et al.[22] for similar carbon-transition metals deposited films (in a-C:Ti and a-C:V samples). This peak should be related to (10) plane of a two-dimensional order in graphenelike regions of the amorphous carbon matrix not forming the crystal carbide. This graphitic region typically appears due to a spontaneous organized nanoscale multilayer growth which has been seen previously in this type of carbon – transition metal depositions with cathodic vacuum arc.

The carbon-zirconium films have a microstructure of crystal nanoclusters or nanoparticles of zirconium carbide embedded in an amorphous carbon matrix (so is more accurate to express as a-C:ZrC). The amorphous character of the carbon has been determined with Raman spectrometry analysis, but results not shown in this work.

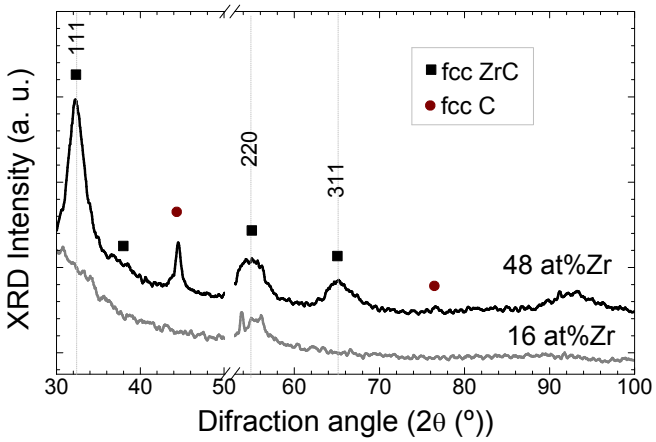

Figure 2. XRD patterns of C:Zr thin films with different metal content. The squares indicate the more important peak position of fcc ZrC

The optical constants of the deposited a-C:ZrC were determined by spectroscopic ellipsometry. All the experimentally measured ellipsometric spectra were fitted with a combination of Drude-type[23] and Tauc-Lorentz [24] dispersion models to merge the metallic behaviour in optical properties of the metallic carbides with the semi-insulating properties observed for the amorphous carbon.

The complex index of refraction of the deposited a-C:ZrC samples with different metal content is represented in Figure 3. The refractive index (n) is very similar for high and low metal content and is found to increase with wavelength, as expected for the metallic behaviour of the layer. However the coefficient of extinction (k), increases for the a-C:ZrC with high Zr content, due is nearly a pure carbide and follows Drude's free-electron model. While the a-C:ZrC with 16 at% Zr, k has a very small value, close to zero, as expected for a dielectric material.

This analysis of the optical constants show that controlling the metal content in the nanocomposite thin film is possible to switch its optical properties as desired for the final application.

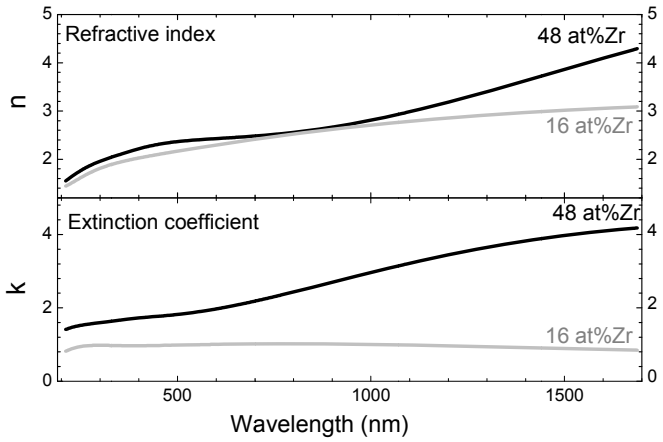

Figure 3.Refractive index (n) and extinction coefficient (k) experimentally determined of C:Zr with two different Zr content.

The tunable optical properties of the a-C:ZrC can be simulated with the software CODE[18]. For that aim, Bruggemann EMA has been employed, where the matrix material is amorphous carbon and the particles embedded are ZrC. The optical constants for both materials employed in the EMA were taken directly from similar FCVA deposited thin films whose optical constants have been calculated previously with spectroscopic ellipsometry.

The complete reflectance spectra (including UV, Vis and NIR wavelength range) were calculated for several combinations of selective coatings. In all, a metallic like infrared reflective layer of ≈300nm is situated between the substrate and the absorber layer. To improve the optical properties, an antireflective layer of ≈60 nm is emplaced at the top of the complete multilayer stack.

For the absorber layer, the previously studied nanocomposite composed with ZrC nanoparticles embedded in a-C matrix was employed. This absorber layer would be composed by only 1, 2 or more layer, with gradient carbide content. Figure 4 show the reflectance spectra calculated for 1 and 2 a-C:ZrC absorber layers. The reflectance spectra have been calculated for 3 and more a-C:ZrC absorber layers, but the absorptance was not improve with more than 2 layers. The absorptance and emittance calculated following equations (2) and (3) for 1 and 2 absorber layers are also shown in the figure. The optimized combination of layers give α= 93.5% and ε_{400}=2.7% for the case of the stack with one a-C:ZrC absorber layer with 77at% of ZrC embedded. This values were improved with the addition of a second absorber layer, obtaining α= 95.4% and ε=3.5% for the case of the selective coating with two a-C:ZrC layers, with optimized thicknesses and carbide content.

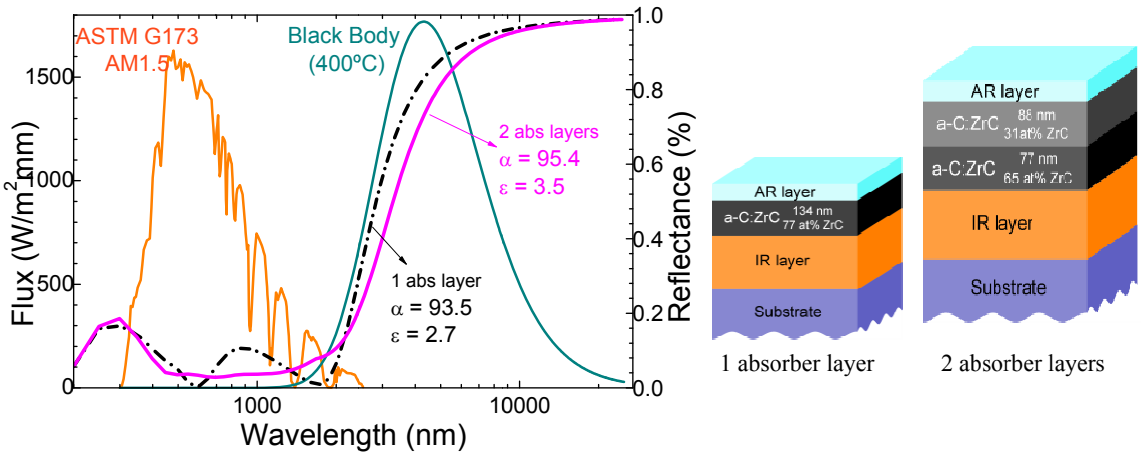

Figure 4.Reflectance spectra of the simulated multilayer varying one in the C:Zr absorber layer: (a) different Zr content and (b) different thickness.

The content of ZrC in the composite material and the thickness of the absorber layer are fluctuated to optimize the optical properties: highest solar absorptance and lowest thermal emittance. Figure 5 shows the variation of these optical properties versus the thickness of upper a-C:ZrC absorber layers, and versus its thickness. The selected values are obtained for the highest solar absorptance. The minimum emittance is reached when there is no layer, or the layer is pure carbon, without carbide what implies a drastic downturn in the thermal stability. Thus a compromise has to be done between α and ε to select the best combination of optical properties.

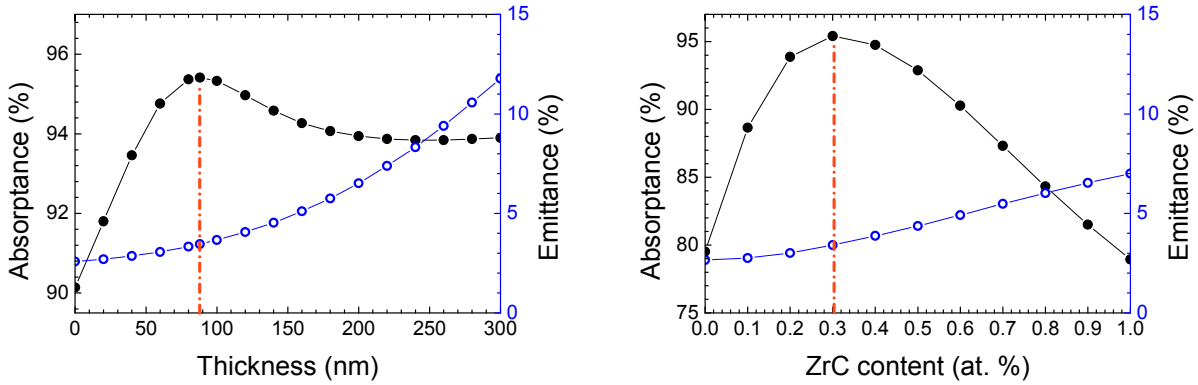

Figure 5. Absorptance and emittance variation versus thickness and carbide content of the a-C:ZrC absorber layer of the complete solar selective coating simulated.

The studied solar selective coating was successfully deposited by filtered cathodic arc technique, adjusting the composition and thicknesses of the simulated complete stack. The cross section SEM image is shown in Figure 6. As can be appreciated in the figure, the deposited films have a very smooth surface with low roughness, thanks to the correct removal of droplets or macroparticles typical of cathodic arc deposition without filter. Additionally, good adhesion between the different layers that compose the coating is observed in the SEM image, with a dense and homogeneous growth along all the solar selective coating.

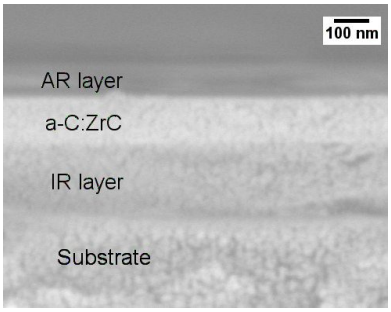

Figure 6. SEM image showing the deposited TiN / C:Zr /Al_2O_3 multilayer on Si substrate.

4. CONCLUSIONS

Carbon and Zirconium cathodes were co-deposited with cathodic vacuum arc technique. The composition, crystal structure and optical properties of the deposited single layers were investigated. The thin films obtained consisted of zirconium carbide nanoparticles embedded in a carbon matrix with different composition as the deposition parameters are varied. The optical properties of the a-C:ZrC can be simulated employing an EMA formula and modulate its absorptive behavior with a variation in the zirconium carbide content in the nanocomposite. A complete solar selective

coating was simulated employing a-C:ZrC thin film as absorber layer, a antireflective layer on the top and an infrared reflective layer between the absorber layer and the substrate. The thickness and carbide content were optimized to obtain a solar absorptance of 95.4% and thermal emittance of 3.4%. The simulated multilayer was deposited with cathodic arc technique. a-C:ZrC nanocomposites are promising materials as solar absorber layers for solar selective coatings.

5. ACKNOWLEDGMENTS

The authors would like to thank Dr. Gintautas Abrasonis for helpful discussion about these materials.

This project was partially support by H2020 project "Framework of Innovation for Engineering of New Durable Solar Surfaces (FRIENDS2)" and Centro para el Desarrollo Tecnológico Industrial (CDTI) project "INvestigación y DEsarrollo de recubrimientos SOLares selectivos de alta temperatura obtenidos mediante técnicas PVD (INDESOL)" IDI-20130896.

Any opinions, findings and conclusions or recommendations expressed in this material are those of the authors and do not necessarily reflect those of the host institutions or funders.

6. REFERENCES

[1] Kennedy, C. E.., Price, H., "Progress in Development of High-Temperature Solar-Selective Coating," Sol. Energy **2005**, 749–755, Asme (2005).

[2] Farooq, M., Green, A. A.., Hutchins, M. G., "High performance sputtered Ni : SiO2 composite solar absorber surfaces," Sol. Energy Mater. Sol. Cells **54**, 67–73 (1998).

[3] Shah, A. a., Ungaro, C.., Gupta, M. C., "High temperature spectral selective coatings for solar thermal systems by laser sintering," Sol. Energy Mater. Sol. Cells **134**, 209–214, Elsevier (2015).

[4] Bittar, A., "Study of TiOxNy thin film selective surfaces produced by ion assisted deposition," J. Vac. Sci. Technol. A Vacuum, Surfaces, Film. **15**(2), 223, AVS: Science & Technology of Materials, Interfaces, and Processing (1997).

[5] Harding, G. L., "Absorptance and emittance of metal carbide selective surfaces sputter deposited onto glass tubes," Sol. Energy Mater. **2**(4), 469–481 (1980).

[6] Zhang, Q.., Mills, D. R., "Very low-emittance solar selective surfaces using new film structures," J. Appl. Phys. **60**(5), 545–547 (1992).

[7] Céspedes, E., Wirz, M., Sánchez-García, J. A., Alvarez-Fraga, L., Escobar-Galindo, R.., Prieto, C., "Novel Mo–Si3N4 based selective coating for high temperature concentrating solar power applications," Sol. Energy Mater. Sol. Cells **122**, 217–225 (2014).

[8] Harding, G. L., "Graded metal carbide solar selective surfaces coated onto glass tubes by a magnetron sputtering system," J. Vac. Sci. Technol. **16**(6), 2101 (1979).

[9] Milde, F., Dimer, M., Hecht, C., Schulze, D.., Gantenbein, P., "Large-area production of solar absorbent multilayers by MF-pulsed plasma technology," Vacuum **59**(2-3), 825–835 (2000).

[10] Mammadov, F., "Study of Selective Surface of Solar Heat Receiver," Int. J. Energy Eng. **2**(4), 138–144 (2012).

[11] Maxwell-Garnett, J. C., "Colours in Metal Glasses, in Metallic Films, and in Metallic Solutions. II," Philos. Trans. R. Soc. A Math. Phys. Eng. Sci. **205**(387-401), 237–288 (1906).

[12] Bruggeman, D., "Calculation of various physics constants in heterogenous substances I Dielectricity constants and conductivity of mixed bodies from isotropic substances," Ann. Phys. **24**(7), 636–664, Wiley-V C H Verlag GMBH (1935).

[13] Bergman, D., "Dielectric - Constant if a Composite material - Problem in classical Physicis," Phys. reports Rev. Sect. Phys. Lett. **43**(9), 378–407 (1978).

[14] Pardo, A., Buijnsters, J. G., Endrino, J. L., Gómez-Aleixandre, C., Abrasonis, G., Bonet, R.., Caro, J., "Effect of the metal concentration on the structural, mechanical and tribological properties of self-organized a-C:Cu hard nanocomposite coatings," Appl. Surf. Sci. **280**, 791–798 (2013).

[15] Mayer, M., SIMNRA User ' s Guide, Max-Plank-Institut für Plasmaphysuk, Garching, Germany (1997).
[16] Abrasonis, G., Oates, T. W. H., Kovács, G. J., Grenzer, J., Persson, P. O. A., Heinig, K.-H. H., Martinavičius, A., Jeutter, N., Baehtz, C., et al., "Nanoscale precipitation patterns in carbon–nickel nanocomposite thin films: Period and tilt control via ion energy and deposition angle," J. Appl. Phys. **108**(4), 043503 (2010).
[17] Woollam, J. A., WVASE Commercial software manual (2000).
[18] Theiss, W., "CODE Manual. Optical Spectrum Simulation" (2007).
[19] ASTM., ASTM G173: "Standard Tables for Reference Solar Spectral Irradiance at Air Mass 1.5: Direct Normal and Hemispherical for a 37 Degree Tilted Surface," 21, US (2008).
[20] Duffie, J. A.., Beckman, W. A., Solar engineering of thermal processes., 3rd ed., John Wiley & Sons, New York (2005).
[21] Wei, S., Hua, H. Z.., Xiang, X., "Thermodynamic Analysis and Growth of Zirconium Carbide by Chemical Vapor Deposition," Phys. Procedia **46**, 88–101 (2013).
[22] Adelhelm, C., Balden, M., Rinke, M.., Stueber, M., "Influence of doping (Ti, V, Zr, W) and annealing on the sp carbon structure of amorphous carbon films," J. Appl. Phys. **105**(3), 033522 (2009).
[23] Modine, F., Haywood, T.., Allison, C., "Optical and electrical properties of single-crystalline zirconium carbide," Phys. Rev. B **32**(12), 7743–7747, American Physical Society (1985).
[24] Jellison, G. E., "Optical functions of GaAs, GaP, and Ge determined by two-channel polarization modulation ellipsometry," Opt. Mater. (Amst). **1**(3), 151–160 (1992).